https://doi.org/10.5194/bg-2019-256
Preprint. Discussion started: 15 July 2019

Biogeosciences Discussions
Open Access
EGU

Leveraging the signature of heterotrophic respiration on atmospheric CO_2 for model benchmarking.

Samantha J. Basile[1], Xin Lin[1] William R. Wieder[2,3], Melannie D. Hartman [2,4], Gretchen Keppel-Aleks[1]

[1] Department of Climate and Space Sciences and Engineering, University of Michigan, Ann Arbor, MI, 48105, USA
[2] Climate and Global Dynamics Laboratory, National Center for Atmospheric Research, Boulder, CO, 80305, USA
[3] Institute of Arctic and Alpine Research, University of Colorado, Boulder, CO, 80309, USA
[4] Natural Resource Ecology Laboratory, Colorado State University, Fort Collins CO, 80523, USA

Correspondence to: Samantha Basile (sjbasile@umich.edu)

Abstract

Spatial and temporal variations in atmospheric carbon dioxide (CO_2) reflect large-scale net carbon exchange between the atmosphere and terrestrial ecosystems. Soil heterotrophic respiration (HR) is one of the component fluxes that drive this net exchange but, given observational limitations, it is difficult to quantify this flux or to evaluate global-scale model simulations thereof. Here, we show that atmospheric CO_2 can provide a useful constraint on large-scale patterns of soil heterotrophic respiration. We analyze three soil model configurations (CASA-CNP, MIMICS and CORPSE) that simulate HR fluxes within a biogeochemical testbed that provides each model with identical net primary productivity (NPP) and climate forcings. We subsequently quantify the effects of variation in simulated terrestrial carbon fluxes (NPP and HR from the three soil testbed models) on atmospheric CO_2 distributions using a three-dimensional atmospheric tracer transport model. Our results show that atmospheric CO_2 observations can be used to identify deficiencies in model simulations of the seasonal cycle and interannual variability in HR relative to NPP. In particular, the two models that explicitly simulated microbial processes (MIMICS and CORPSE) were more variable than observations at interannual timescales and showed a stronger than observed temperature sensitivity. Our results prompt future research directions to use atmospheric CO_2, in combination with additional constraints on terrestrial productivity or soil carbon stocks, for evaluating HR fluxes.

https://doi.org/10.5194/bg-2019-256
Preprint. Discussion started: 15 July 2019

1. Introduction

Atmospheric CO_2 observations reflect net exchange of carbon between the land and oceans with the atmosphere. Observations of atmospheric CO_2 concentration have been collected *in situ* since the late 1950s (Keeling et al., 2011), and global satellite observations have become available within the last decade (Crisp et al., 2017; Yokota et al., 2009). The high precision and accuracy of *in situ* observations and the fact that these measurements integrate information about ecosystem carbon fluxes over a large concentration footprint make atmospheric CO_2 a strong constraint on model predictions of net carbon exchange (Keppel-Aleks et al., 2013). For example, at seasonal timescales, atmospheric CO_2 can be used to evaluate the growing-season net flux, especially in the Northern Hemisphere (Yang et al., 2007). At interannual timescales, variations in the atmospheric CO_2 growth rate are primarily driven by changes in terrestrial carbon fluxes in response to climate variability (Cox et al., 2013; Humphrey et al., 2018; Keppel-Aleks et al., 2014). Recent studies have hypothesized that soil carbon processes represent one of the key processes in driving these interannual variations (Cox et al., 2013; Wunch et al, 2013). Moreover, soil carbon processes represent one of the largest uncertainties in predicting future carbon-climate feedbacks, in part because non-permafrost soils contain an estimated 1500 to 2400 PgC (Bruhwiler et al., 2018), at least a factor of three larger than the pre-industrial atmospheric carbon reservoir.

Soil heterotrophic respiration (HR), the combination of litter decay and microbial breakdown of organic matter, is the main pathway for CO_2 release from soil carbon pools to the atmosphere. Currently, insights on HR rates and controls are mostly derived from local-scale observations. For example, soil chamber observations can be used to measure soil respiration (which includes root and heterotrophic respiration fluxes) at spatial scales on the order of 100 cm^2 (Davidson et al., 2002; Pumpanen et al., 2004; Ryan and Law, 2005). Ecosystem respiration (combined autotrophic and heterotrophic respiration fluxes) can also be backed out from eddy covariance net ecosystem exchange observations at spatial scales around 1 km^2, but with substantial uncertainty (Baldocchi 2008; Barba et al., 2018; Lavigne et al., 1997). Because fine-scale variations in environmental drivers such as soil type and soil moisture affect rates of HR, it is difficult to scale local respiration observations to zonal or global scales. Even with use of advanced techniques such as artificial neural networks, lack of information for remote or under-

https://doi.org/10.5194/bg-2019-256
Preprint. Discussion started: 15 July 2019

sampled zones contributes uncertainty to bottom-up HR estimates (Bond-Lamberty et al., 2018; Zhao et al, 2017).

Local-scale observations reveal that HR is sensitive to numerous climate drivers, including temperature, moisture, and freeze-thaw state (Baldocchi 2008; Barba et al., 2018; Lavigne et al., 1997). Because of these links to climate, predicting the evolution of HR and soil carbon stocks within coupled Earth system models is necessary for climate predictions. Within prognostic models, heterotrophic respiration has been represented as a first-order decay process based on precipitation, temperature, and a linear relationship with available substrate (Jenkinson et al., 1990; Parton, 1993, Randerson et al., 1996). However, such representations may neglect key processes for the formation of soil and persistence of soil organic carbon (SOC) stocks (Lehmann and Kleber 2015; Schmidt et al. 2011; Rasmussen et al. 2018). More recently, models have begun to explicitly represent microbial processes into global-scale simulations of the formation and turnover of litter and SOC (Sulman et al., 2014; Wieder et al., 2013) as well as to evaluate microbial trait-based signatures on SOC dynamics (Wieder et al., 2015). These advances in the representation of SOC formation and turnover increase capacities to test emerging ideas about soil C persistence and vulnerabilities, but also increase the uncertainties in how to implement and parameterize these theories in models (Bradford et al. 2016; Sulman et al. 2018; Wieder et al. 2018).

Given these uncertainties, developing methods to benchmark model representations of HR fluxes is an important research goal (Bond-Lamberty et al. 2018b) as model predictions for soil carbon change over the 21st century are highly uncertain (Schuur et al., 2018; Todd-Brown et al., 2014). A common method for model evaluation is to directly compare spatial or temporal variations in model properties (e.g., leaf area index) or processes (e.g., gross primary productivity) against observations (Randerson 2009; Turner et al., 2006). Such comparisons assess model fidelity under present day climate, but may not ensure future predictivity of the model. The use of functional response metrics, which evaluate the relationship between a model process and an underlying driver, may ensure that the model captures the sensitivities required to predict future evolution (Collier 2018, Keppel-Aleks et al., 2018). A third benchmarking approach is to use hypothesis-driven approaches or experimental manipulations to evaluate processes (Medlyn et

https://doi.org/10.5194/bg-2019-256
Preprint. Discussion started: 15 July 2019

al., 2015). It is likely that these methods will have maximum utility when combined within a benchmarking framework (e.g., Collier, 2018; Hoffman et al., 2016) since they evaluate different aspects of model predictive capability.

Here, we hypothesize that atmospheric CO_2 data can be used to evaluate simulations of soil heterotrophic respiration and differentiate between the chemical and microbial parameterizations used in state-of-the-art models. Previous work has shown that atmospheric CO_2 observations are inherently sensitive to HR across a range of timescales. For example, at seasonal timescales, improving the parameterization for litterfall in the CASA model improved its phasing of the simulated atmospheric CO_2 annual cycle (Randerson et al., 1996). At interannual timescales, variations in the Northern Hemisphere CO_2 seasonal minimum are hypothesized to arise from variations in respiration (Wunch et al., 2013) and variations in the growth rate have been linked to tropical respiration and its temperature sensitivity (Anderegg et al., 2015). In this analysis, we simulate atmospheric CO_2 distributions using three different soil model representations that are part of a soil biogeochemical testbed (Wieder et al., 2018). The three sets of HR fluxes, were shown in Wieder et al., (2018) to have distinct patterns at seasonal timescales, are used as boundary conditions for a 3-dimensional atmospheric transport model. We evaluate temporal variability in the resulting CO_2 simulations against observations, quantify the functional relationships between CO_2 variability and temperature variability, and quantify the regional influences of land carbon fluxes on global CO_2 variability. The methods and results are presented in Section 2 and 3, and discussion of the implications for benchmarking and our understanding of drivers of atmospheric CO_2 variability are presented in Section 4.

2. Data and Methods

2.1 Observations and timeseries analysis

For this analysis we use reference CO_2 measurements from 34 marine boundary layer sites (MBL, Table S1) within the NOAA Earth System Research Laboratory sampling network (ESRL, Fig. 1; Dlugokencky et al., 2016). These sites were chosen to minimize the influence of local anthropogenic emissions and had at least 50% data coverage over the 29-year period between 1982 and 2010. We detrend all timeseries data using a third-order polynomial fit to remove the impact of annually increasing atmospheric concentration in our seasonal and

https://doi.org/10.5194/bg-2019-256
Preprint. Discussion started: 15 July 2019

interannual calculations (SFig. 1). Using the detrended CO_2 data, we calculate a period median annual cycle by averaging all observations for a given calendar month. To calculate CO_2 interannual variability (CO_2 IAV), the median annual cycle is subtracted from the detrended timeseries (SFig. 1, Fig. 4). We diagnose the magnitude of CO_2 IAV using one standard deviation, unless otherwise noted. Model simulated CO_2 seasonality and interannual variability is calculated using the same methods.

Following the approach in Keppel-Aleks et al., 2018, we aggregate site specific CO_2 by averaging measurement timeseries across six latitude zones (Fig.1, solid lines): Northern Hemisphere high latitudes (61 to 90°N), midlatitudes (24 to 60°N), tropics (1 to 23°N), Southern Hemisphere tropics (0 to 23°S), and extratropics (24 to 60°S and 61 S to 90 S). The global mean CO_2 timeseries is constructed as an area-weighted average of these six atmospheric zones.

2.2 Soil testbed representations of heterotrophic respiration

We used a soil biogeochemical testbed (Wieder et al., 2018), which generates daily estimates of soil carbon stocks and fluxes at global scale without the computational burden of running a full land model. The testbed is a chain of model simulations where soil models with different structures can be run under the same forcing data, including the same net primary productivity (NPP) fluxes, soil temperature, and soil moisture. Each testbed soil model in this analysis produces unique gridded heterotrophic respiration (HR) values based on its own underlying mechanism and soil C stocks. Currently, we are running with a carbon-only configuration of the testbed. From the testbed output we calculate the net ecosystem productivity (NEP) as the difference between HR and NPP, specifically HR-NPP, to account for the opposite sign convention between the component fluxes.

For the simulations described in this paper, the chain starts with the Community Land Model 4.5 (CLM4.5; Oleson et al., 2013), run with satellite phenology with CRU-NCEP climate reanalysis as forcing data (Jones et al., 2013; Kalnay et al., 1996; Le Quéré et al., 2018). In this simplified formulation of CLM, a single plant functional type is assumed in each 2° by 2° gridcell. Daily values for gross primary productivity (GPP), soil moisture, soil temperature, and air temperature from CLM4.5 are passed to the Carnegie-Ames Stanford Approach terrestrial model (CASA-

https://doi.org/10.5194/bg-2019-256
Preprint. Discussion started: 15 July 2019

CNP; Potter et al. 1993; Randerson et al., 1996; Randerson et al., 1997; Wang et al., 2010). The CASA-CNP plant model uses the data from CLM4.5 to calculate NPP and carbon allocation to roots, wood, and leaves. This module also determines the timing of litterfall. Finally, metabolic litter, structural litter, and decomposing coarse woody debris (CWD) are then passed to the soil biogeochemical models.

The three soil models make distinct assumptions about microbial processes. More details regarding these formulations and their implementation in the testbed are found in Wieder et al. (2018), but we provide brief descriptions here. The CASA-CNP soil model computes first-order, linear decay rates modified by soil temperature and moisture, implicitly representing microbial activity and soil carbon turnover through a cascade of organic matter pools (CASA: Randerson et al., 1997; CASA-CNP: CASA carbon cycling with additional nitrogen, and phosphorus cycling, Wang et al. 2010). These include metabolic and structural litter, as well as a fast, slow, and passive soil carbon pools. The Microbial-Mineralization Carbon Stabilization model (MIMICS; Wieder et al., 2014; Wieder et al., 2015) explicitly represents microbial activity with a temperature-sensitive reverse Michaelis-Menten kinetics (Buchkowski et al., 2017; Moorhead and Weintraub, 2018) but has no soil moisture controls. The decomposition pathway is set up with two litter pools (identical to those simulated by CASA-CNP), three soil organic matter pools (available, chemically and physically protected), and two microbial biomass pools for copiotrophic (fast) and oligotrophic (slow) microbial functional groups. The Carbon, Organisms, Rhizosphere, and Protection in the Soil Environment model (CORPSE) is also microbially explicit and uses reverse Michaelis-Menten kinetics, but it assumes different microbial and soil carbon pools. Surface litter and soil C pools are considered separately, but only soil C has a parallel set of physically protected pools that are isolated from microbial decomposition. CORPSE includes a temperature dependent Maximum Reaction Velocity (V_{max}) parameter, but also includes a term for the soil moisture controls on decomposition rates that uses volumetric liquid soil water content. For all three models, soil texture inputs were also derived from the CLM surface data set (Oleson et al., 2013). We acknowledge that one potential limitation of the approach is a lack of vertical resolution in terms of temperature or frozen fraction of soil moisture (Koven et al. 2013).

https://doi.org/10.5194/bg-2019-256
Preprint. Discussion started: 15 July 2019

While this modeling approach contains necessary simplifications, it provides the ability to query the role of structure in driving differences in fluxes. Model output includes daily net primary production (NPP) from CASA-CNP and HR simulated by CASA-CNP, CORPSE and MIMICS. Daily fluxes between 1982 and 2010 are averaged to monthly values and masked into land regions that align with the CO_2 sampling zones (section 2.1, Fig. 1, color fill): Northern Hemisphere high latitudes (NHL; 61 to 90°N), midlatitudes (NML; 24 to 60°N), tropics (NT; 1 to 23°N), Southern Hemisphere tropics (ST; 0 to 23°S), and extratropics (SE; 24 to 90°S) – here the two Southern Hemisphere extratropical regions were combined into one flux area since Antarctic carbon fluxes are negligible. Land-area integrated flux timeseries are then used for seasonal and interannual calculations (method described in section 2.1). However, the raw daily fluxes between 1980 and 2010 are used as boundary conditions to an atmospheric transport model, again separated by latitude zones listed above, to simulate the imprint of these different soil model configurations on monthly atmospheric CO_2.

2.3 GEOS-Chem atmospheric transport modeling of CO_2

We simulate the imprint of the testbed fluxes on atmospheric CO_2 using GEOS-Chem, a 3-D atmospheric transport model. We run the GEOS-Chem v12.0.0 CO_2 simulation between 1980 and 2010 at a resolution of 2.0° in latitude by 2.5° in longitude with 47 vertical levels. The model is driven by hourly meteorological fields from the Modern-Era Retrospective analysis for Research and Application version 2 (MERRA2) reanalysis data (Gelaro et al., 2017; https://gmao.gsfc.nasa.gov/reanalysis/MERRA-2/), with the dynamic timestep set to be 600 seconds. The model is initialized with a globally-uniform atmospheric CO_2 mole fraction equal to 350 ppm. Results of the first two years (1980 and 1981) are reserved for model spin-up, and we analyze the monthly average outputs for the period 1982–2010. To minimize influence of land-atmosphere boundary layer dynamics and the influence of anthropogenic emissions, we sample the resulting GEOS-Chem simulations at the 3rd vertical level for grid cell points with latitude and longitude values closest to 34 marine boundary layer (MBL) sites within the NOAA ESRL network. We calculated the latitude zone averaging, median annual cycle and interannual variability calculations using the methods described for observed CO_2 (see section 2.1). Aggregating CO_2 from individual sites is consistent with our hypothesis that atmospheric CO_2 may provide constraints on large-scale, rather than local, patterns of heterotrophic respiration. As

https://doi.org/10.5194/bg-2019-256
Preprint. Discussion started: 15 July 2019

such, averaging simulated and observed CO_2 across latitude zones smooths local information while retaining information about regional scale fluxes.

We isolate the imprint of NPP and three representations of HR on the spatial and temporal evolution of atmospheric CO_2 by using daily testbed results as boundary conditions (section 2.2). We also separately tag CO_2 originating from the five flux zones delineated in the previous section (Fig. 1). Overall, we track 20 CO_2 tracers in total (4 sets of fluxes and 5 flux regions) within the GEOS-Chem model. Throughout the manuscript, we refer to CO_2 originating from these NPP and HR component fluxes as CO_2^{NPP} and CO_2^{HR}, respectively. For the atmospheric CO_2 simulations, we used the sign convention that a positive flux indicates a flux into the atmosphere. Therefore, CO_2^{NEP}, indicating CO_2 from net ecosystem production (NEP), is calculated from the addition of CO_2^{NPP} and CO_2^{HR}. The same notation will be used to denote the testbed ensemble sources. For example, CO_2^{HR} simulated from CORPSE fluxes is defined as $CO_2^{CORPSE\ HR}$, similarly for $CO_2^{CORPSE\ NEP}$. We note that the net CO_2 response from the model (i.e., CO_2^{NEP}) is approximately equivalent to observations in terms of seasonal and interannual variations, although we neglect ocean fluxes and emissions from fossil fuels, land use and land cover change, and fire. Previous studies have demonstrated that NEP drives most of the atmospheric CO_2 seasonality (> 90%; Nevison et al., 2008; Randerson et al., 1997) and interannual variability (e.g., Rayner et al. 2008; Battel et al. 2000).

2.4 Global temperature sensitivity and separation of regional influences

For insight on a functional climate response, we investigate the global temperature sensitivity of the atmospheric CO_2 growth rate and the testbed ensemble fluxes. Variability in the CO_2 growth rate anomaly was calculated as the difference between timestep *n* and *n*-1 for the monthly and annual interannual variability (IAV) timeseries. Testbed flux timeseries were averaged to monthly resolution and interpolated (averaged between months) to match the monthly initiation of each corresponding CO_2 growth rate anomaly timeseries. Following Arora et al. (2013), we calculate temperature sensitivity (γ) using an ordinary linear regression for the timeseries of temperature interannual variability (T IAV) with 1) atmospheric CO_2 growth rate anomalies, and 2) land flux IAV (see section 2.2). For atmospheric CO_2 growth rate anomalies, each timeseries was converted from ppm y^{-1} to PgC y^{-1} based on the global mass of atmospheric dry air. Thus, all

https://doi.org/10.5194/bg-2019-256
Preprint. Discussion started: 15 July 2019

global sensitivity values are reported in units of PgC y^{-1} K^{-1}. A reference global temperature sensitivity value for the CO_2 growth rate was calculated for 1982 to 2010 using ESRL CO_2 observations and the Climatic Research Unit's gridded temperature product (CRU TS4; Jones et al., 2012). The CRU TS4 historical product was used because it consists of directly interpolated station data.

We also assess the influence of individual regions on the global mean signal for both component land fluxes (NPP, HR) and simulated atmospheric CO_2 (CO_2^{NPP}, CO_2^{HR}, CO_2^{NEP}). To quantify each region's contribution to global variability we calculate the ratio of regional IAV magnitude to global IAV magnitude, which we define as relative standard deviation (σ_{REL}). For each flux and CO_2 region (NHL, NML, NT, ST, SE), this ratio is calculated from the standard deviation of each monthly IAV timeseries. However, for the regional values of simulated CO_2 IAV, we identify the global mean response to a single region's fluxes. That is, the CO_2 IAV averaged across all six CO_2 regions but sourced only from testbed fluxes in the NHL, or NML, etc., without influence from the other flux regions. We then take the standard deviation of this regionally-selected global mean IAV for the ratio to total global CO_2 IAV magnitude (derived from all global fluxes). To measure the strength of each region's impact on global values, we use the same regional-global partitioning to calculate correlation coefficients (r) for the timeseries of component flux IAV and CO_2 IAV. Thus, if an individual region were responsible for all observed global flux or CO_2 variability, it would have both σ_{REL} and r values equal to 1 in this comparison. The value for σ_{REL} decreases with the magnitude of regional variability, and r decreases if the variability is not coherent with the global signal, even if the magnitude of variability is high.

3. Results

3.1 Seasonal imprint of heterotrophic respiration

The three soil carbon models in the testbed impart different fingerprints on atmospheric CO_2 variability. Both CO_2^{NPP} and CO_2^{HR} show largest seasonality in the NHL, with seasonal amplitudes decaying toward the tropics and Southern Hemisphere. In the NHL, the peak-to-trough amplitude of CO_2^{NPP} is 39±2 ppm, with a seasonal maximum in April and a seasonal minimum in August (Fig. 2a). The seasonal cycles for CO_2^{HR} simulated from all testbed models

https://doi.org/10.5194/bg-2019-256
Preprint. Discussion started: 15 July 2019

are out of phase with that of CO_2^{NPP}, and there are large amplitude differences in CO_2^{HR} among the model ensemble members. Specifically, the NHL amplitude of $CO_2^{CORPSE\ HR}$ is 28±3 ppm, while the amplitudes for $CO_2^{MIMICS\ HR}$ and $CO_2^{CASA\text{-}CNP\ HR}$ are only 17±1 ppm, accounting for about 40-70% of the amplitude from CO_2^{NPP} (Table 1). However, in all latitude bands, the largest CO_2^{HR} amplitude comes from the microbially explicit models – CORPSE for the Northern Hemisphere and MIMICS for the Southern Hemisphere (Table 1). The amplitudes of CO_2^{NPP} and CO_2^{HR} decrease further south, but the amplitude ratio of CO_2^{HR} to CO_2^{NPP} in NML and NT remains about 0.4-0.7 (Fig. 2b-c; Table 1). In the Southern Hemisphere tropics, the amplitude of CO_2^{NPP} was smaller than that the Northern Hemisphere, however amplitude of CO_2^{HR} was similar to the NT values (Table 1). In the Southern Hemisphere extratropics, the amplitudes for all components were less 3 ppm (Table 1).

The phasing of CO_2^{HR} is an important driver of the overall comparison between CO_2^{NEP} and observed CO_2 seasonality (Fig. 3). When the contributions of NPP and HR seasonality are considered together (i.e., CO_2^{HR} + CO_2^{NPP}), the simulated amplitude of CO_2^{NEP} is larger than the observed CO_2 across all latitude bands (Fig. 3). The largest mismatch is in the NHL zone, where the observed mean annual cycle is 15±0.9 ppm, while the peak-to-trough CO_2^{NEP} ranges from 23±1.3 ppm for CORPSE to 33±1.4 ppm for MIMICS (Fig. 3a). The smaller CO_2^{NEP} amplitude simulated by CORPSE is due to the large CO_2^{HR} seasonality that counteracts the seasonality in NPP (Fig. 2a-b). Furthermore, $CO_2^{MIMICS\ HR}$ and $CO_2^{CASA\text{-}CNP\ HR}$ have similar amplitudes in the NHL (Fig. 2a; Table 1), but the CO_2^{NEP} amplitude from these two models differs (33±1.2 ppm versus 26±1 ppm, respectively; Fig. 3a; Table 1). This occurs because $CO_2^{MIMICS\ HR}$ peaks one-month later than $CO_2^{CASA\text{-}CNP\ HR}$, and has a zero-crossing that is more closely aligned with the trough of CO_2^{NPP} (Fig. 2a), leading to the larger amplitude in $CO_2^{MIMICS\ NEP}$ (Fig. 3a; Table 1). Although the amplitude mismatch decreases towards the south (Fig. 3b-f), the overall bias in the Northern Hemisphere suggests that either the seasonality of NPP is too large, or that all testbed models underestimate the seasonality of HR. Within the ST region, ensemble CO_2^{HR} minima are opposite to that in CO_2^{NPP}, leading to a small annual cycle in simulations whereas the double peak in the ESRL observations may reflect fluxes not accounted for in our framework (Figs. 2d, 3d).

https://doi.org/10.5194/bg-2019-256
Preprint. Discussion started: 15 July 2019

3.2 Interannual imprint of heterotrophic respiration

The testbed ensemble reasonably simulates the magnitude and timing of interannual variability (IAV) compared with CO_2 observations (Fig. 4). Across the six latitude bands analyzed, simulated CO_2^{NEP} IAV generally falls within one standard deviation of the median variation from observations for most of the study period (Fig. 4). Taking a closer look at the CO_2 from the component fluxes (NPP and HR), across all six latitude bands, the CO_2^{NPP} IAV standard deviation is between 0.9 and 1.1 ppm for component fluxes (Fig. 5a). $CO_2^{CASA\text{-}CNP\ HR}$ IAV shows similar standard deviation as CO_2^{NPP} IAV, whereas the standard deviations of $CO_2^{CORPSE\ HR}$ and $CO_2^{MIMICS\ HR}$ range from 0.7-1.4 ppm and 0.5-1.1 ppm, respectively (Fig. 5a). Combining the CO_2 responses from component fluxes to CO_2^{NEP} reveals a latitudinal gradient in IAV standard deviation similar to that of ESRL observations, with largest standard deviation found in the northern extratropics (Fig. 5b). Among the three testbed models, the standard deviation of $CO_2^{CASA\ NEP}$ agrees best with observations across all latitude bands ($CO_2^{CASA\ NEP}$: 0.5-0.9 ppm; ESRL: 0.6-1.0 ppm; Fig. 5b). $CO_2^{CORPSE\ NEP}$ overestimates IAV by up to 30% in NHL and NML, but agrees better with observations in the tropics and Southern Hemisphere. $CO_2^{MIMICS\ NEP}$ overestimates IAV standard deviations across all latitude bands (Fig. 5b). Interestingly, in the NHL, the overestimation is 20% even though $CO_2^{MIMICS\ HR}$ shows similar IAVs as CO_2^{NPP} (both 1.1 ppm; Fig.5). This suggests that the phasing of $CO_2^{MIMICS\ HR}$ IAV relative to CO_2^{NPP} contributes to $CO_2^{MIMICS\ NEP}$ bias.

Both global NPP and HR fluxes are sensitive to temperature variations at interannual timescales, with increased build-up of CO_2 in the atmosphere at higher temperatures. Since these temperature sensitivities cannot be directly constrained from observations, we calculate temperature sensitivities for the CO_2 resulting from these component fluxes as well as from NEP. For CASA-CNP, the temperature sensitivity (γ) for globally integrated NPP and HR fluxes is 2.5 PgC yr^{-1} K^{-1} and 1.7 PgC yr^{-1} K^{-1}; respectively (Fig. 6a). The temperature sensitivity of HR was higher for the microbially explicit models: 2.1 PgC yr^{-1} K^{-1} for CORPSE and 4.2 PgC yr^{-1} K^{-1} for MIMICS (Fig. 6a). For any given testbed flux (NPP, HR, or NEP), the temperature sensitivity of the resulting global mean CO_2 growth rate anomaly is higher than that of the underlying flux IAV. For example, the temperature sensitivity of the globally integrated NPP flux IAV (γNPP) is 2.5 PgC yr^{-1} K^{-1} whereas γCO_2^{NPP} is 3.2 PgC yr^{-1} K^{-1}. The apparent

https://doi.org/10.5194/bg-2019-256
Preprint. Discussion started: 15 July 2019

amplification of the temperature sensitivity was even larger for HR. For example, the temperature sensitivity of MIMICS HR IAV (γHR^{MIMICS}) was 4.2 PgC yr^{-1} K^{-1}, whereas $\gamma CO_2^{MIMICS\ HR}$ was 7.7 PgC yr^{-1} K^{-1} (Fig. 6a). The resulting testbed CO_2^{NEP} overestimates the temperature sensitivity of the observed atmospheric CO_2 growth rate anomaly (6.1±2.5 PgC yr^{-1} K^{-1}; Fig. 6b). CASA-CNP and CORPSE have temperature sensitivities within the range of the observed sensitivity, but $\gamma CO_2^{MIMICS\ NEP}$ is 80% larger than observed value (10.9 PgC yr^{-1} K^{-1}; Fig. 6b). We note that the γHR and γCO_2^{HR} is an emergent property that reflects both direct and indirect temperature influences, including the impact of temperature variability on NPP and litterfall (Table S3).

3.3 Geographic origins of CO_2 IAV

The interannual variability (IAV) in global NPP and HR originate from different geographic regions. The IAV in global NPP fluxes are dominated by variations within the NT and ST regions, with relative standard deviation σ_{REL} ~ 0.5 and correlation coefficient r ~ 0.6 (Fig. 7a-b). The NML region also has a similar contribution to the NT in magnitude, but with a lower timing coherence (r = 0.44; Fig. 7a-b). In contrast to the dominance of the tropics in IAV of global NPP, the NML region contributes most to IAV in global HR, with $\sigma_{REL} \geq 0.6$ and r ~ 0.8 for all three testbed models (Fig. 7c-d). The NHL region is also important in driving global HR flux variability based on CORPSE model results (σ_{REL} = 0.59 and r = 0.82; Fig. 7c-d). Despite high NPP variability in the tropics, the magnitude of tropical HR variability is only about 10-30% of global HR variability, and the timing coherence with the global signal is generally low (r < 0.45; Fig. 7a-b). MIMICS HR IAV is the exception for the ST measuring close to 40% of global HR IAV magnitude and relatively high correlation (r = 0.58; Fig. 7a-b). Together, the tropics and NML contribute roughly equally to the magnitude of global NEP variability (σ_{REL} between 0.44-0.55; Fig. 7e). Although the NML and NT show relatively high timing coherence (0.41-0.55), the ST shows the strongest timing coherence with global NEP IAV (r > 0.7; Fig. 7f).

Atmospheric transport modifies patterns of IAV in fluxes, emphasizing tropical flux patterns and de-emphasizing northern hemisphere flux patterns. For example, the role of ST in driving global CO_2^{NPP} variability is amplified compared to the underlying fluxes, as the timing coherence with the global signal increases from r = 0.64 for flux IAV to r = 0.88 for CO_2^{NPP} IAV for this region

https://doi.org/10.5194/bg-2019-256
Preprint. Discussion started: 15 July 2019

(Fig. 7b). Conversely, the role of NML is dampened, with timing coherence decreasing to r = 0.33 for CO_2^{NPP} IAV versus r = 0.44 for NPP IAV (Fig. 7b). Similarly, timing coherence for tropical CO_2^{HR} IAV is substantially higher than that for HR fluxes in ST and NT (>0.7), although the atmospheric transport impact differs across the three testbed models (Fig. 7d). In contrast to closely aligned NML correlation values for CO_2^{HR} and HR (r ~ 0.8-0.9), NML CO_2^{HR} IAV shows σ_{REL} between 0.45 and 0.58, a decrease from the HR IAV contribution (NML HR IAV σ_{REL} range: 0.57 to 0.74; Fig. 7c). For CO_2^{NEP} IAV, the regional contribution is more consistent with similar σ_{REL} and r to flux IAV (Fig. 7e-f).

4. Discussion

Modeled differences in heterotrophic respiration impart discernible signatures on atmospheric CO_2. We analyzed the atmospheric CO_2 response to soil heterotrophic respiration (HR) using a soil testbed ensemble with three plausible representations of HR (CASA-CNP, CORPSE, MIMICS) and a 3-D atmospheric transport model. Results show that HR phasing is important for ecosystem carbon flux (NEP) at both seasonal and interannual timescales. Regional patterns of HR variability provide non-negligible contributions to global CO_2 variability. Here we discuss these findings in more detail as well as implications for the use of CO_2 observations for flux evaluation and model benchmarking.

4.1 Impacts of heterotrophic respiration on seasonality

Our evaluation of CO_2 simulated using testbed fluxes revealed that all testbed models overestimated the mean annual cycle amplitude of atmospheric CO_2 observations. In the Northern Hemisphere, the bias was largest for MIMICS, as the $CO_2^{MIMICS\ NEP}$ amplitude was overestimated by up to 100% (Fig. 3). The mismatch was smallest in $CO_2^{CORPSE\ NEP}$, which was within 70% of the observed annual cycle amplitude where CORPSE simulates the largest seasonal HR fluxes (Fig. 3a-c, Table1). We note that the mismatch across all three testbed formulations could be due to overestimation of the NPP flux used by all three testbed models, or underestimation of HR seasonality. However, an advantage of the testbed approach is that, because all of the models are driven by the same NPP and climate variables, the differences in the HR flux amplitudes arise from structural differences in the testbed. In the Southern Hemisphere, in contrast to the large differences found in the Northern Hemisphere, the simulated

https://doi.org/10.5194/bg-2019-256
Preprint. Discussion started: 15 July 2019

CO_2 annual cycle amplitudes were similar across all three models, with small absolute mismatches (about 1 ppm) compared to observations.

One challenge in using atmospheric CO_2 to evaluate HR representation in soil models is the influence of productivity (NPP) on both HR fluxes and atmospheric CO_2 variations. The seasonal diagnostics we present are very sensitive to the phasing of HR fluxes relative to NPP. For example, in NHL a one-month lag in the seasonal maximum of CO_2^{HR} between MIMICS and CASA-CNP (Fig. 2) leads to a 7 ppm difference in the overall amplitude of CO_2^{NEP}— this despite identical amplitudes of CO_2^{HR} for the two models (Fig. 3). Although the substantial impacts of subtle phase differences complicate benchmarking, the sensitivity reveals interesting and important differences related to model structural choices (i.e. first order versus microbially explicit). Wieder et al., (2018) noted that the microbially explicit models in the testbed had seasonal HR fluxes that peaked in the fall, about a month later than the HR fluxes simulated by CASA-CNP. The timing of CASA-CNP fluxes largely depend on soil temperature (highest HR flux when temperature is highest), whereas MIMICS and CORPSE have maximum HR fluxes set by trade-offs between the timing of maximal temperature and maximal microbial biomass, which is more tightly linked with litterfall (Fig. 7 from Wieder et al., 2018). Thus, phasing of HR is a sensitive diagnostic for benchmarking, especially if additional constraints on the magnitude and phasing of NPP are available.

In this study, determining the unique contribution from HR was possible since NPP was common among the three soil models used in the testbed, but the contribution of NPP will need to be resolved for model evaluation in other contexts. Long-term records of vegetation productivity at regional and global scales have been observed via satellite vegetation indices (Hicke et al., 2002; Meroni et al., 2009; Running et al., 2004), and more recently chlorophyll fluorescence (Frankenberg et al., 2011; Guan et al., 2016; Kohler et al., 2018; Li et al., 2018). Our study underscores the importance of developing methods to use these datasets together with atmospheric CO_2 to inform the dynamics of carbon cycling and its component fluxes.

4.2 Impacts of heterotrophic respiration on interannual variability

https://doi.org/10.5194/bg-2019-256
Preprint. Discussion started: 15 July 2019

Similar to the analyses on seasonal cycles, the testbed ensemble simulations showed a higher CO_2 IAV associated with explicit microbial representation (Fig. 5). This is especially true for CO_2^{CORPSE} in the NHL and NML (Fig. 5a). Interestingly, in the tropics and SE, $CO_2^{MIMICS\ HR}$ IAV is only slightly higher than that of $CO_2^{CASA\text{-}CNP\ HR}$ or $CO_2^{CORPSE\ HR}$, but IAV of $CO_2^{MIMICS\ NEP}$ was 20-30% higher than that of other models. Further, in these regions MIMICS HR IAV also shows an inverse, but highly correlated relationship with NPP IAV ($R^2 > 0.60$, Table S3). This suggests that the large IAV of $CO_2^{MIMICS\ NEP}$ may result from differences in phasing between NPP and MIMICS HR fluxes, similar to phasing between MIMICS NPP and HR affecting the shape of the CO_2^{NEP} annual cycle in NHL. In the NHL, all testbed models show HR IAV is correlated with both NPP IAV and temperature IAV (R^2 of 0.32 to 0.77; Table S3). Additionally, NPP IAV is sensitive to temperature variability ($\gamma = 0.15$, $R^2 = 0.43$; Table S3). Thus better diagnostics for atmospheric CO_2 IAV owing to HR requires additional constraints on NPP fluxes, especially at high latitudes.

The high IAV in $CO_2^{MIMICS\ NEP}$ is consistent with this model having the highest global temperature sensitivity overestimating observed value by 80% (Fig. 6b). CORPSE, the other microbially explicit model, had a 30% higher temperature sensitivity in CO_2^{NEP} than observed globally (Fig. 6b). This large bias in temperature sensitivity demonstrates the structural uncertainty associated with current HR parameterization, and highlights the need for continued investigation of model microbial representation to improve the functional relationship with temperature in soil models.

4.3 Implications for model benchmarking using atmospheric CO_2

Our results provide useful insights for model benchmarking using atmospheric CO_2. On a global scale, interannual variability (IAV) of simulated atmospheric CO_2 was shown to be affected by the variability in component fluxes (NPP, HR) from different land regions (Figs. 5-7). The tropics dominate IAV in global NPP, while northern extratropics dominate the IAV in global HR (Fig. 7a-d). Taken together, NEP variability reflects roughly equal contributions from northern hemisphere temperate ecosystems (NML) and tropical ecosystems (NT and ST; Fig. 7e-f). These results suggest that the interannual variability of atmospheric CO_2 results from two different processes (respiration and productivity) across multiple ecoclimate regions, whereas previous

https://doi.org/10.5194/bg-2019-256
Preprint. Discussion started: 15 July 2019

studies have mostly identified tropical (e.g. Cox et al., 2013; Wang et al., 2013) or subtropical, semi-arid regions (e.g. Ahlstorm et al., 2015; Poulter et al., 2014) as dominant controls on the global CO_2 IAV.

Our analysis underscores that patterns of variability in atmospheric CO_2 are tied not only to variabilities in the underlying fluxes, but also to atmospheric transport. For example, we showed that the temperature sensitivity of CO_2 growth rate anomalies was larger than the sensitivity estimated from the fluxes themselves (Fig. 6). The enhanced temperature sensitivity for CO_2^{HR} was larger than for that of CO_2^{NPP}, which suggests that the geographic origin of the fluxes relative to dominant patterns of transport affects the result (Fig. 6a). This transport enhancement of the apparent temperature sensitivity of CO_2 growth rate anomalies is consistent with results from Keppel-Aleks et al. (2018). While these results may be tied to the choice of GEOS-Chem to simulate atmospheric transport, they do underscore that (1) atmospheric CO_2 must be simulated from land fluxes to be use as a benchmark and (2) atmospheric observations should not be assumed to be a direct proxy for fluxes themselves.

We employed several benchmarking approaches, including timeseries comparison and functional response to temperature, to evaluate if CO_2 patterns reflect underlying representations of soil heterotrophic respiration. We found that soil heterotrophic respiration leaves non-negligible imprints on atmospheric CO_2, leaving open the possibility of more explicitly accounting for respiration variability using atmospheric CO_2 observations. Given that HR links to NPP, soil C pools, and temperature, we recommend synergistically using datasets that reflect these variables (instead of identifying metrics in isolation). This could provide better model process evaluation if implemented in a larger benchmarking framework, such as the International Land Model Benchmarking Project (ILAMB; Collier, 2018; Hoffman et al., 2016). Model development will be crucial in the next decade of carbon cycle research, but so will tools to test mechanistic understanding and elucidate a coherent picture of the land-atmosphere carbon response to a changing climate.

https://doi.org/10.5194/bg-2019-256
Preprint. Discussion started: 15 July 2019

Code and Data Availability

NOAA Earth System Research Laboratory CO_2 measurements (Dlugokencky et al., 2016; ftp://aftp.cmdl.noaa.gov/data/trace_gases/co2/flask/surface/) and the Climatic Research Unit's gridded temperature product (Jones et al., 2012; http://badc.nerc.ac.uk/view/badc.nerc.ac.uk__ATOM__ACTIVITY_0c08abfc-f2d5-11e2-a948-00163e251233) are publicly available online. CASA testbed information and fluxes have been previously published in Wieder et al., 2018. GEOSChem CO_2 response data is available at the University of Michigan Library Deep Blue online repository (Basile et al., 2019; https://deepblue.lib.umich.edu/data/concern/data_sets/gt54kn02m).

Author Contributions

Samantha J. Basile and Gretchen Keppel-Aleks designed the research. William R. Wieder, Melannie D. Hartman, and Xin Lin contributed model components. Samantha J. Basile conducted the analysis. All authors contributed to discussions. Samantha Basile wrote the manuscript

Competing Interests

The authors declare that they have no conflict of interest.

Acknowledgements

Funding for this work was provided through the NASA ROSES Interdisciplinary Science Grant NNX17AK19G and through the RUBISCO Science Focus Area sponsored by the DoE Regional and Global Model Analysis program. We thank NOAA ESRL for providing observations of atmospheric CO_2. We thank the Climate Research Unit for their historically gridded temperature product.

References

Ahlström, A., Raupach, M., Schurgers, G., Smith, B., Arneth, A., Jung, M., Reichstein, M., Canadell, J., Friedlingstein, P., Jain, A., Kato, E., Poulter, B., Sitch, S., Stocker, B., Viovy, N., Wang, Y. P., Wiltshire, A., Zaehle, S. and Zeng, N.: The dominant role of semi-arid ecosystems in the trend and variability of the land CO_2 sink, Science (80-.)., 348(6237), 895–899, doi:10.1002/2015JA021022, 2015.

https://doi.org/10.5194/bg-2019-256
Preprint. Discussion started: 15 July 2019

Arora, V. K., Boer, G. J., Friedlingstein, P., Eby, M., Jones, C. D., Christian, J. R., Bonan, G., Bopp, L., Brovkin, V., Cadule, P., Hajima, T., Ilyina, T., Lindsay, K., Tjiputra, J. F. and Wu, T.: Carbon-concentration and carbon-climate feedbacks in CMIP5 earth system models, J. Clim., 26(15), 5289–5314, doi:10.1175/JCLI-D-12-00494.1, 2013.

Baldocchi, D.: TURNER REVIEW No. 15. "Breathing" of the terrestrial biosphere: Lessons learned from a global network of carbon dioxide flux measurement systems, Aust. J. Bot., 56(1), 1–26, doi:10.1071/BT07151, 2008.

Barba, J., Cueva, A., Bahn, M., Barron-Gafford, G. A., Bond-Lamberty, B., Hanson, P. J., Jaimes, A., Kulmala, L., Pumpanen, J., Scott, R. L., Wohlfahrt, G. and Vargas, R.: Comparing ecosystem and soil respiration: Review and key challenges of tower-based and soil measurements, Agric. For. Meteorol., 249(August 2017), 434–443, doi:10.1016/j.agrformet.2017.10.028, 2018.

Basile, S., Lin, X., Keppel-Aleks, G.: Simulated CO_2 dataset using the atmospheric transport model GEOSChem v12.0.0: Response to regional land carbon fluxes, https://doi.org/10.7302/xjzc-xy05, 2019.

Bond-Lamberty, B.: New Techniques and Data for Understanding the Global Soil Respiration Flux, Earth's Futur., 6(9), 1176–1180, doi:10.1029/2018EF000866, 2018.

Bond-Lamberty, B. and Thomson, A.: A global database of soil respiration data, Biogeosciences, 7(6), 1915–1926, doi:10.5194/bg-7-1915-2010, 2010.

Bond-Lamberty, B., Bailey, V. L., Chen, M., Gough, C. M. and Vargas, R.: Globally rising soil heterotrophic respiration over recent decades, Nature, 560(7716), 80–83, doi:10.1038/s41586-018-0358-x, 2018.

Bradford, M. A., Wieder, W. R., Bonan, G. B., Fierer, N., Raymond, P. A. and Crowther, T. W.: Managing uncertainty in soil carbon feedbacks to climate change, Nat. Clim. Chang., 6(8), 751–758, doi:10.1038/nclimate3071, 2016.

Bruhwiler, L., Michalak, A. M., Birdsey, R., Huntzinger, D. N., Fisher, J. B., Miller, J. and Houghton, R. A.: Overview of the Global Carbon Cycle, Second State Carbon Cycle Rep., 1–33, doi:10.7930/SOCCR2.2018.Ch1, 2018.

Buchkowski, R. W., Bradford, M. A., Grandy, A. S., Schmitz, O. J. and Wieder, W. R.: Applying population and community ecology theory to advance understanding of belowground biogeochemistry, Ecol. Lett., 20(2), 231–245, doi:10.1111/ele.12712, 2017.

Collier, N., Hoffman, F. M., Lawrence, D. M., Keppel-Aleks, G., Koven, C. D., Riley, W. J., Mu, M. and Randerson, J. T.: The International Land Model Benchmarking (ILAMB) System: Design, Theory, and Implementation, J. Adv. Model. Earth Syst., 10(11), 2731–2754, doi:10.1029/2018MS001354, 2018.

https://doi.org/10.5194/bg-2019-256
Preprint. Discussion started: 15 July 2019

Collins, W., Deaven, D., Gandin, L., Iredell, M., Jenne, R. and Joseph, D.: The NCEP NCAR 40-Year Reanalysis Project, Bull. Am. Meteorol. Soc., 77(3), 437–472, doi:10.1175/JCLI-D-16-0758.1, 1996.

Cox, P. M., Pearson, D., Booth, B. B., Friedlingstein, P., Huntingford, C., Jones, C. D. and Luke, C. M.: Sensitivity of tropical carbon to climate change constrained by carbon dioxide variability., Nature, 494(7437), 341–4, doi:10.1038/nature11882, 2013.

Crisp, D., Pollock, H., Rosenberg, R., Chapsky, L., Lee, R., Oyafuso, F., Frankenberg, C., Dell, C., Bruegge, C., Doran, G., Eldering, A., Fisher, B., Fu, D., Gunson, M., Mandrake, L., Osterman, G., Schwandner, F., Sun, K., Taylor, T., Wennberg, P. and Wunch, D.: The on-orbit performance of the Orbiting Carbon Observatory-2 (OCO-2) instrument and its radiometrically calibrated products, Atmos. Meas. Tech., 10(1), 59–81, doi:10.5194/amt-10-59-2017, 2017.

Davidson, E. A., Savage, K., Verchot, L. V. and Navarro, R.: Minimizing artifacts and biases in chamber-based measurements of soil respiration, Agric. For. Meteorol., 113(1–4), 21–37, doi:10.1016/S0168-1923(02)00100-4, 2002.

Dlugokencky, E. J., Lang P. M., Mund J. W., Crotwell A. M., Crotwell M. J., and Thoning K. W.: Atmospheric carbon dioxide dry air mole fractions from the NOAA ESRL carbon cycle cooperative global air sampling network, 1968–2015, version 2016-08-30. NOAA, accessed 4 January 2017, ftp://aftp.cmdl.noaa.gov/data/trace_gases/co2/flask/surface/, 2016.

Frankenberg, C., Fisher, J. B., Worden, J., Badgley, G., Saatchi, S. S., Lee, J. E., Toon, G. C., Butz, A., Jung, M., Kuze, A. and Yokota, T.: New global observations of the terrestrial carbon cycle from GOSAT : Patterns of plant fluorescence with gross primary productivity, , 38, 1–6, doi:10.1029/2011GL048738, 2011.

Gelaro, R., McCarty, W., Suárez, M. J., Todling, R., Molod, A., Takacs, L., Randles, C. A., Darmenov, A., Bosilovich, M. G., Reichle, R., Wargan, K., Coy, L., Cullather, R., Draper, C., Akella, S., Buchard, V., Conaty, A., da Silva, A. M., Gu, W., Kim, G. K., Koster, R., Lucchesi, R., Merkova, D., Nielsen, J. E., Partyka, G., Pawson, S., Putman, W., Rienecker, M., Schubert, S. D., Sienkiewicz, M. and Zhao, B.: The modern-era retrospective analysis for research and applications, version 2 (MERRA-2), J. Clim., 30(14), 5419–5454, doi:10.1175/JCLI-D-16-0758.1, 2017.

Guan, K., Berry, J. A., Zhang, Y., Joiner, J., Guanter, L., Badgley, G. and Lobell, D. B.: Improving the monitoring of crop productivity using spaceborne solar-induced fluorescence, Glob. Chang. Biol., 22(2), 716–726, doi:10.1111/gcb.13136, 2016.

Hicke, J. A., Asner, G. P., Randerson, J. T., Tucker, C., Los, S., Birdsey, R., Jenkins, J. C. and Field, C.: Trends in North American net primary productivity derived from satellite observations, 1982-1998, Global Biogeochem. Cycles, 16(2), 2-1-2–14, doi:10.1029/2001gb001550, 2002.

Hoffman, F. M., Koven, C. D., Keppel-Aleks, G., Lawrence, D. M., Riley, W. J., Randerson, J.

https://doi.org/10.5194/bg-2019-256
Preprint. Discussion started: 15 July 2019

T., Ahlström, A., Abramowitz, G., Baldocchi, D. D., Best, M. J., Bond-Lamberty, B., De Kauwe, M. G., Denning, A. S., Desai, A. R., Eyring, V., Fisher, J. B., Fisher, R. A., Gleckler, P. J., Huang, M., Hugelius, G., Jain, A. K., Kiang, N. Y., Kim, H., Koster, R. D., Kumar, S. V., Li, H., Luo, Y., Mao, J., McDowell, N. G., Mishra, U., Moorcroft, P. R., Pau, G. S. H., Ricciuto, D. M., Schaefer, K., Schwalm, C. R., Serbin, S. P., Shevliakova, E., Slater, A. G., Tang, J., Williams, M., Xia, J., Xu, C., Joseph, R. and Koch, D.: 2016 International Land Model Benchmarking (ILAMB) Workshop Report, , doi:10.2172/1330803, 2017.

Humphrey, V., Zscheischler, J., Ciais, P., Gudmundsson, L., Sitch, S. and Seneviratne, S. I.: Sensitivity of atmospheric CO_2 growth rate to observed changes in terrestrial water storage, Nature, 560(7720), 628–631, doi:10.1038/s41586-018-0424-4, 2018.

Jenkinson, A. D. S., Andrew, S. P. S., Lynch, J. M., Goss, M. J., Tinker, P. B. and Jenkinson, D. S.: The turnover of organic carbon and nitrogen in soil, Philos. Trans. R. Soc. London. Ser. B Biol. Sci., 329(1255), 361–368, doi:10.1098/rstb.1990.0177, 1990.

Jiang, L., Ji, D., Luo, Y., Liang, J., Xia, J., Li, Z., Wang, Y.-P., Rinke, A., Zhang, G., Ahlström, A., Koven, C., Chen, G., McGuire, A. D., Ciais, P., Peng, S., Hayes, D. J., Shi, Z., Krinner, G., Dong, J., Moore, J. C., Yan, L., Cheng, W. and Xiao, X.: Non-uniform seasonal warming regulates vegetation greening and atmospheric CO 2 amplification over northern lands , Environ. Res. Lett., 13(12), 124008, doi:10.1088/1748-9326/aae9ad, 2018.

Jones, P., and Harris, I.: CRU TS3. 21: Climatic Research Unit (CRU) Time-Series (TS) version 3.21 of high resolution gridded data of month-by-month variation in climate (Jan. 1901–Dec. 2012). NCAS British Atmospheric Data Centre, http://badc.nerc.ac.uk/view/badc.nerc.ac.uk__ATOM__ACTIVITY_0c08abfc-f2d5-11e2-a948-00163e251233, doi:10.5285/D0E1585D-3417-485F-87AE-4FCECF10A992, 2013.

Jones, P. D., Lister, D. H., Osborn, T. J., Harpham, C., Salmon, M. and Morice, C. P.: Hemispheric and large-scale land-surface air temperature variations: An extensive revision and an update to 2010, J. Geophys. Res. Atmos., 117(5), doi:10.1029/2011JD017139, 2012.

Keeling, C. D., Piper, S. C., Whorf, T. P. and Keeling, R. F.: Evolution of natural and anthropogenic fluxes of atmospheric CO 2 from 1957 to 2003, Tellus, Ser. B Chem. Phys. Meteorol., 63(1), 1–22, doi:10.1111/j.1600-0889.2010.00507.x, 2011.

Keppel-Aleks, G., Randerson, J. T., Lindsay, K., Stephens, B. B., Keith Moore, J., Doney, S. C., Thornton, P. E., Mahowald, N. M., Hoffman, F. M., Sweeney, C., Tans, P. P., Wennberg, P. O. and Wofsy, S. C.: Atmospheric carbon dioxide variability in the community earth system model: Evaluation and transient dynamics during the twentieth and twenty-first centuries, J. Clim., 26(13), 4447–4475, doi:10.1175/JCLI-D-12-00589.1, 2013.

Keppel-Aleks, G., Wolf, A. S., Mu, M., Doney, S. C., Morton, D. C., Kasibhatla, P. S., Miller, J. B., Dlugokencky, E. J. and Randerson, J. T.: Small phytoplankton drive high summertime carbon and nutrient export in the Gulf of California and Eastern Tropical North Pacifi, Global Biogeochem. Cycles, 29, 1295–1310, doi:10.1002/2014GB004890.Received, 2014.

https://doi.org/10.5194/bg-2019-256
Preprint. Discussion started: 15 July 2019

Keppel-Aleks, G., Basile, S. J. and Hoffman, F. M.: A functional response metric for the temperature sensitivity of tropical ecosystems, Earth Interact., 22(7), doi:10.1175/EI-D-17-0017.1, 2018.

Konings, A. G., Bloom, A. A., Liu, J., Parazoo, N. C., Schimel, D. S. and Bowman, K. W.: Global, Satellite-Driven Estimates of Heterotrophic Respiration, Biogeosciences Discuss., 2100(November), 1–26, doi:10.5194/bg-2018-466, 2018.

Koven, C. D., Riley, W. J., Subin, Z. M., Tang, J. Y., Torn, M. S., Collins, W. D., Bonan, G. B., Lawrence, D. M. and Swenson, S. C.: The effect of vertically resolved soil biogeochemistry and alternate soil C and N models on C dynamics of CLM4, Biogeosciences, 10(11), 7109–7131, doi:10.5194/bg-10-7109-2013, 2013.

Lavigne, M. B., Ryan, M. G., Anderson, D. E., Baldocchi, D. D., Crill, P. M., Fitzjarrald, D. R., Goulden, M. L., Gower, S. T., Massheder, J. M., McCaughey, J. H., Rayment, M. and Striegl, R. G.: Comparing nocturnal eddy covariance measurements to estimates of ecosystem respiration made by scaling chamber measurements at six coniferous boreal sites, J. Geophys. Res. Atmos., 102(D24), 28977–28985, doi:10.1029/97jd01173, 1997.

Lehmann, J. and Kleber, M.: The contentious nature of soil organic matter, Nature, 528(7580), 60–68, doi:10.1038/nature16069, 2015.

Medlyn, B. E., Zaehle, S., De Kauwe, M. G., Walker, A. P., Dietze, M. C., Hanson, P. J., Hickler, T., Jain, A. K., Luo, Y., Parton, W., Prentice, I. C., Thornton, P. E., Wang, S., Wang, Y. P., Weng, E., Iversen, C. M., Mccarthy, H. R., Warren, J. M., Oren, R. and Norby, R. J.: Using ecosystem experiments to improve vegetation models, Nat. Clim. Chang., 5(6), 528–534, doi:10.1038/nclimate2621, 2015.

Meroni, M., Rossini, M., Guanter, L., Alonso, L., Rascher, U., Colombo, R. and Moreno, J.: Remote sensing of solar-induced chlorophyll fluorescence: Review of methods and applications, Remote Sens. Environ., 113(10), 2037–2051, doi:10.1016/j.rse.2009.05.003, 2009.

Moorhead, D. L. and Weintraub, M. N.: The evolution and application of the reverse Michaelis-Menten equation, Soil Biol. Biochem., 125(May), 261–262, doi:10.1016/j.soilbio.2018.07.021, 2018.

Myneni, R. B., Canadell, J. G., White, M. A., Nemani, R. R., Sitch, S., Ciais, P., Wang, W., Hashimoto, H., Milesi, C. and Piao, S.: Variations in atmospheric CO_2 growth rates coupled with tropical temperature, Proc. Natl. Acad. Sci., 110(32), 13061–13066, doi:10.1073/pnas.1219683110, 2013.

Nevison, C. D., Mahowald, N. M., Doney, S. C., Lima, I. D., van der Werf, G. R., Randerson, J. T., Baker, D. F., Kasibhatla, P. and McKinley, G. A.: Contribution of ocean, fossil fuel, land biosphere, and biomass burning carbon fluxes to seasonal and interannual variability in atmospheric CO_2, J. Geophys. Res. Biogeosciences, 113(1), 1–21, doi:10.1029/2007JG000408, 2008.

https://doi.org/10.5194/bg-2019-256
Preprint. Discussion started: 15 July 2019

Oleson, K. W., Lawrence, D. M., Bonan, G. B., Drewniak, B., Huang, M., Charles, D., Levis, S., Li, F., Riley, W. J., Zachary, M., Swenson, S. C., Thornton, P. E., Bozbiyik, A., Fisher, R., Heald, C. L., Kluzek, E., Lamarque, F., Lawrence, P. J., Leung, L. R., Muszala, S., Ricciuto, D. M. and Sacks, W.: Technical description of version 4.5 of the Community Land Model (CLM), NCAR Technical Note NCAR/TN-503+STR, Natl. Cent. Atmos. Res. Boulder, CO, (July), 420pp, doi:10.5065/D6RR1W7M, 2013.

Parton, W. J.: The CENTURY Model, in: Evaluation of Soil Organic Matter Models, edited by: Powlson, D. S., Smith, P. and Smith, J. U., Springer-Verlag, Berlin, Heidelberg, Germany, 283–291, 1996.

Potter, C. S., Randerson, J. T., Field, C. B., Matson, P. A., Vitousek, P. M., Mooney, H. A., and Klooster, S. A.: Terrestrial ecosystem production: A process model based on global satellite and surface data, Global Biogeochem. Cycles, 7(4), 811–841, doi:10.1029/93GB02725, 1993.

Poulter, B., Frank, D., Ciais, P., Myneni, R.B., Andela, N., Bi, J., Broquet, G., Canadell, J.G., Chevallier, F., Liu, Y.Y., Running, S.W., Stich, S. and van der Werf, G.R.: Contribution of semi-arid ecosystems to interannual variability of the global carbon cycle, Nature, 509(7502), 600–603, doi:10.1038/nature13376, 2014.

Pumpanen, J., Kolari, P., Ilvesniemi, H., Minkkinen, K., Vesala, T., Niinistö, S., Lohila, A., Larmola, T., Morero, M., Pihlatie, M., Janssens, I., Yuste, J. C., Grünzweig, J. M., Reth, S., Subke, J. A., Savage, K., Kutsch, W., Østreng, G., Ziegler, W., Anthoni, P., Lindroth, A. and Hari, P.: Comparison of different chamber techniques for measuring soil CO 2 efflux, Agric. For. Meteorol., 123(3–4), 159–176, doi:10.1016/j.agrformet.2003.12.001, 2004.

Le Quéré, C., Andrew, R. M., Friedlingstein, P., Sitch, S., Pongratz, J., Manning, A. C., Korsbakken, J. I., Peters, G. P., Canadell, J. G., Jackson, R. B., Boden, T. A., Tans, P. P., Andrews, O. D., Arora, V. K., Bakker, D. C. E., Barbero, L., Becker, M., Betts, R. A., Bopp, L., Chevallier, F., Chini, L. P., Ciais, P., Cosca, C. E., Cross, J., Currie, K., Gasser, T., Harris, I., Hauck, J., Haverd, V., Houghton, R. A., Hunt, C. W., Hurtt, G., Ilyina, T., Jain, A. K., Kato, E., Kautz, M., Keeling, R. F., Klein Goldewijk, K., Körtzinger, A., Landschützer, P., Lefèvre, N., Lenton, A., Lienert, S., Lima, I., Lombardozzi, D., Metzl, N., Millero, F., Monteiro, P. M. S., Munro, D. R., Nabel, J. E. M. S., Nakaoka, S., Nojiri, Y., Padín, X. A., Peregon, A., Pfeil, B., Pierrot, D., Poulter, B., Rehder, G., Reimer, J., Rödenbeck, C., Schwinger, J., Séférian, R., Skjelvan, I., Stocker, B. D., Tian, H., Tilbrook, B., van der Laan-Luijkx, I. T., van der Werf, G. R., van Heuven, S., Viovy, N., Vuichard, N., Walker, A. P., Watson, A. J., Wiltshire, A. J., Zaehle, S. and Zhu, D.: Global Carbon Budget 2017, Earth Syst. Sci. Data Discuss., 1–79, doi:10.5194/essd-2017-123, 2018.

Randerson, J. T., Hoffman, F. M., Thornton, P. E., Mahowald, N. M., Lindsay, K., Lee, Y. H., Nevison, C. D., Doney, S. C., Bonan, G., Stöckli, R., Covey, C., Running, S. W. and Fung, I. Y.: Systematic assessment of terrestrial biogeochemistry in coupled climate-carbon models, Glob. Chang. Biol., 15(10), 2462–2484, doi:10.1111/j.1365-2486.2009.01912.x, 2009.

https://doi.org/10.5194/bg-2019-256
Preprint. Discussion started: 15 July 2019

Randerson, J. T., Thompson, M. V., Conway, T. J., Fung, I. Y. and Field, C. B.: The contribution of sources and sinks to trends in the seasonal cycle of atmospheric carbon dioxide, Global Biogeochem. Cycles, 11(4), 535–560, doi:10.1029/97GB02268, 1997.

Randerson, J. T., Thompson, M. V., Malmstrom, C. M.: Substrate Limitations for Heterotrophs: Implications for models that estimate the seasonal cycle of atmospheric CO_2, Global Biogeochem. Cycles, 10(4), 585–602, doi:10.1029/96GB01981, 1996.

Rasmussen, C., Heckman, K., Wieder, W. R., Keiluweit, M., Lawrence, C. R., Berhe, A. A., Blankinship, J. C., Crow, S. E., Druhan, J. L., Hicks Pries, C. E., Marin-Spiotta, E., Plante, A. F., Schädel, C., Schimel, J. P., Sierra, C. A., Thompson, A. and Wagai, R.: Beyond clay: towards an improved set of variables for predicting soil organic matter content, Biogeochemistry, 137(3), 297–306, doi:10.1007/s10533-018-0424-3, 2018.

Rayner, P. J., Law, R. M., Allison, C. E., Francey, R. J., Trudinger, C. M. and Pickett-Heaps, C.: Interannual variability of the global carbon cycle (1992-2005) inferred by inversion of atmospheric CO 2 and δ 13 CO 2 measurements, Global Biogeochem. Cycles, 22(3), 1–12, doi:10.1029/2007GB003068, 2008.

Rienecker, M. M., Suarez, M. J., Gelaro, R., Todling, R., Bacmeister, J., Liu, E., Bosilovich, M. G., Schubert, S. D., Takacs, L., Kim, G. K., Bloom, S., Chen, J., Collins, D., Conaty, A., Da Silva, A., Gu, W., Joiner, J., Koster, R. D., Lucchesi, R., Molod, A., Owens, T., Pawson, S., Pegion, P., Redder, C. R., Reichle, R., Robertson, F. R., Ruddick, A. G., Sienkiewicz, M. and Woollen, J.: MERRA: NASA's modern-era retrospective analysis for research and applications, J. Clim., 24(14), 3624–3648, doi:10.1175/JCLI-D-11-00015.1, 2011.

Running, S. W., Nemani, R. R., Heinsch, F. A., Zhao, M., Reeves, M. and Hashimoto, H.: A Continuous Satellite-Derived Measure of Global Terrestrial Primary Production, Bioscience, 54(6), 547, doi:10.1641/0006-3568(2004)054[0547:ACSMOG]2.0.CO;2, 2004.

Ryan, M. G. and Law, B. E.: Interpreting, measuring, and modeling soil respiration, Biogeochemistry, 73(1), 3–27, doi:10.1007/s10533-004-5167-7, 2005.

Schmidt, M. W. I., Torn, M. S., Abiven, S., Dittmar, T., Guggenberger, G., Janssens, I. A., Kleber, M., Kögel-Knabner, I., Lehmann, J., Manning, D. A. C., Nannipieri, P., Rasse, D. P., Weiner, S. and Trumbore, S. E.: Persistence of soil organic matter as an ecosystem property., Nature, 478(7367), 49–56, doi:10.1038/nature10386, 2011.

Sulman, B. N., Phillips, R. P., Oishi, A. C., Shevliakova, E. and Pacala, S. W.: Microbe-driven turnover offsets mineral-mediated storage of soil carbon under elevated CO 2, Nat. Clim. Chang., 4(12), 1099–1102, doi:10.1038/nclimate2436, 2014.

Sulman, B. N., Moore, J. A. M., Abramoff, R., Averill, C., Kivlin, S., Georgiou, K., Sridhar, B., Hartman, M. D., Wang, G., Wieder, W. R., Bradford, M. A., Luo, Y., Mayes, M. A., Morrison, E., Riley, W. J., Salazar, A., Schimel, J. P., Tang, J. and Classen, A. T.: Multiple models and experiments underscore large uncertainty in soil carbon dynamics, Biogeochemistry, 141(2),

https://doi.org/10.5194/bg-2019-256
Preprint. Discussion started: 15 July 2019

109–123, doi:10.1007/s10533-018-0509-z, 2018.

Todd-Brown, K. E. O., Randerson, J. T., Hopkins, F., Arora, V., Hajima, T., Jones, C., Shevliakova, E., Tjiputra, J., Volodin, E., Wu, T., Zhang, Q. and Allison, S. D.: Changes in soil organic carbon storage predicted by Earth system models during the 21st century, Biogeosciences, 11(8), 2341–2356, doi:10.5194/bg-11-2341-2014, 2014.

Turner, D. P., Ritts, W. D., Cohen, W. B., Gower, S. T., Running, S. W., Zhao, M., Costa, M. H., Kirschbaum, A. A., Ham, J. M., Saleska, S. R. and Ahl, D. E.: Evaluation of MODIS NPP and GPP products across multiple biomes, Remote Sens. Environ., 102(3–4), 282–292, doi:10.1016/j.rse.2006.02.017, 2006.

Wang, Y. P., Law, R. M. and Pak, B.: A global model of carbon, nitrogen and phosphorus cycles for the terrestrial biosphere, Biogeosciences, 7(7), 2261–2282, doi:10.5194/bg-7-2261-2010, 2010.

Wieder, W. R., Bonan, G. B. and Allison, S. D.: Global soil carbon projections are improved by modelling microbial processes, Nat. Clim. Chang., 3(10), 909–912, doi:10.1038/nclimate1951, 2013.

Wieder, W. R., Grandy, A. S., Kallenbach, C. M. and Bonan, G. B.: Integrating microbial physiology and physio-chemical principles in soils with the MIcrobial-MIneral Carbon Stabilization (MIMICS) model, Biogeosciences, 11(14), 3899–3917, doi:10.5194/bg-11-3899-2014, 2014.

Wieder, W. R., Grandy, A. S., Kallenbach, C. M., Taylor, P. G. and Bonan, G. B.: Representing life in the Earth system with soil microbial functional traits in the MIMICS model, Geosci. Model Dev., 8(6), 1789–1808, doi:10.5194/gmd-8-1789-2015, 2015.

Wieder, W. R., Hartman, M. D., Sulman, B. N., Wang, Y. P., Koven, C. D. and Bonan, G. B.: Carbon cycle confidence and uncertainty: Exploring variation among soil biogeochemical models, Glob. Chang. Biol., 24(4), 1563–1579, doi:10.1111/gcb.13979, 2018.

Wunch, D., Wennberg, P. O., Messerschmidt, J., Parazoo, N. C., Toon, G. C., Deutscher, N. M., Keppel-Aleks, G., Roehl, C. M., Randerson, J. T., Warneke, T. and Notholt, J.: The covariation of Northern Hemisphere summertime CO_2 with surface temperature in boreal regions, Atmos. Chem. Phys., 13(18), 9447–9459, doi:10.5194/acp-13-9447-2013, 2013.

Yokota, T., Yoshida, Y., Eguchi, N., Ota, Y., Tanaka, T., Watanabe, H. and Maksyutov, S.: Global Concentrations of CO_2 and CH_4 Retrieved from GOSAT: First Preliminary Results, Sola, 5, 160–163, doi:10.2151/sola.2009-041, 2009.

Zhao, Z., Peng, C., Yang, Q., Meng, F. R., Song, X., Chen, S., Epule, T. E., Li, P. and Zhu, Q.: Model prediction of biome-specific global soil respiration from 1960 to 2012, Earth's Futur., 5(7), 715–729, doi:10.1002/2016EF000480, 2017.

https://doi.org/10.5194/bg-2019-256
Preprint. Discussion started: 15 July 2019

Table 1 Atmospheric CO_2 mean annual cycle amplitude (in ppm) simulated from heterotrophic respiration (HR), net primary productivity (NPP), and net ecosystem productivity (NEP). The median annual cycle amplitudes for observed CO_2 (CO_2^{OBS}) averaged over latitude bands are also reported.

	NHL 61°-90°N	**NML** 24°-60°N	**NT** 0°-23°N	**ST** 1°-23°S	**SE** 24°-60°S	**SE** 61°-90°S
$CO_2^{CASA\text{-}CNP\ HR}$	17.6	11.4	4.3	4.3	1.1	1.9
$CO_2^{CORPSE\ HR}$	28.2	16.6	6.4	4.9	1.4	2.2
$CO_2^{MIMICS\ HR}$	17.2	11.8	5.1	4.4	1.9	2.5
$CO_2^{CASA\text{-}CNP\ NPP}$	39.3	24.6	11.9	6.0	3.1	3.1
$CO_2^{CASA\text{-}CNP\ NEP}$	26.2	16.3	9.3	1.6	2.2	2.2
$CO_2^{CORPSE\ NEP}$	23.4	14.8	8.7	1.3	2.2	2.4
$CO_2^{MIMICS\ NEP}$	32.8	19.0	10.4	1.7	1.9	2.1
CO_2^{OBS}	15.3	10.6	6.1	0.9	0.8	1.4

https://doi.org/10.5194/bg-2019-256
Preprint. Discussion started: 15 July 2019

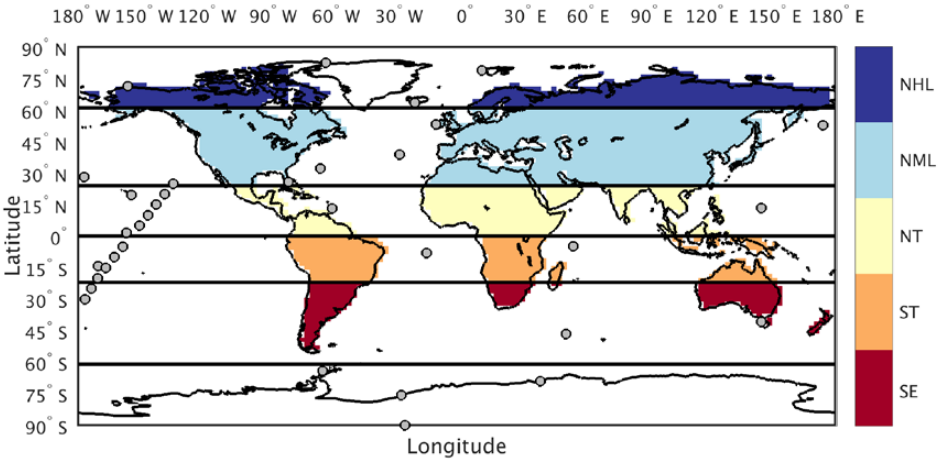

Figure 1. Tagged flux regions and marine boundary layer CO_2 observing sites used in our analysis. The 5 tagged flux regions are shown in color fill: Northern High Latitude (NHL), Northern Mid-Latitude (NML), Northern Tropics (NT), Southern Tropics (ST) and Southern Extratropics (SE). For sampling simulated CO_2 consistent with the tagged flux regions, we aggregate marine boundary layer sites (filled circles) into 6 latitude bands defined by the black lines.

https://doi.org/10.5194/bg-2019-256
Preprint. Discussion started: 15 July 2019

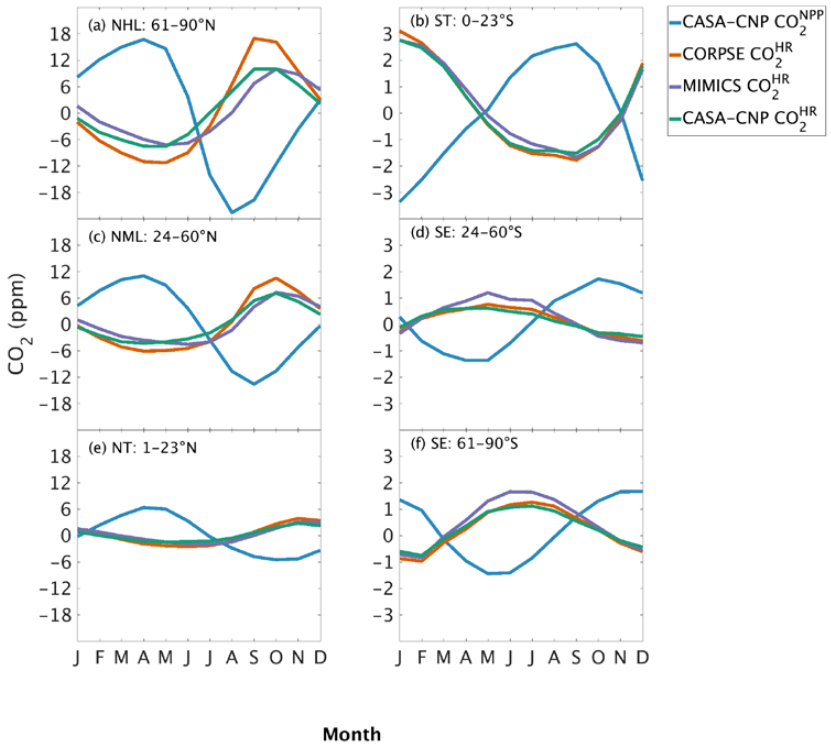

Figure 2: Climatological annual cycle (median) of atmospheric CO_2 simulated from individual flux components (CO_2^{NPP}, CO_2^{HR}) between 1982 and 2010 for atmospheric sampling bands in the Northern Hemisphere (a-c) and Southern Hemisphere (d-f). Note the change in y-axis scale between the two hemispheres.

https://doi.org/10.5194/bg-2019-256
Preprint. Discussion started: 15 July 2019

Biogeosciences
Discussions
Open Access

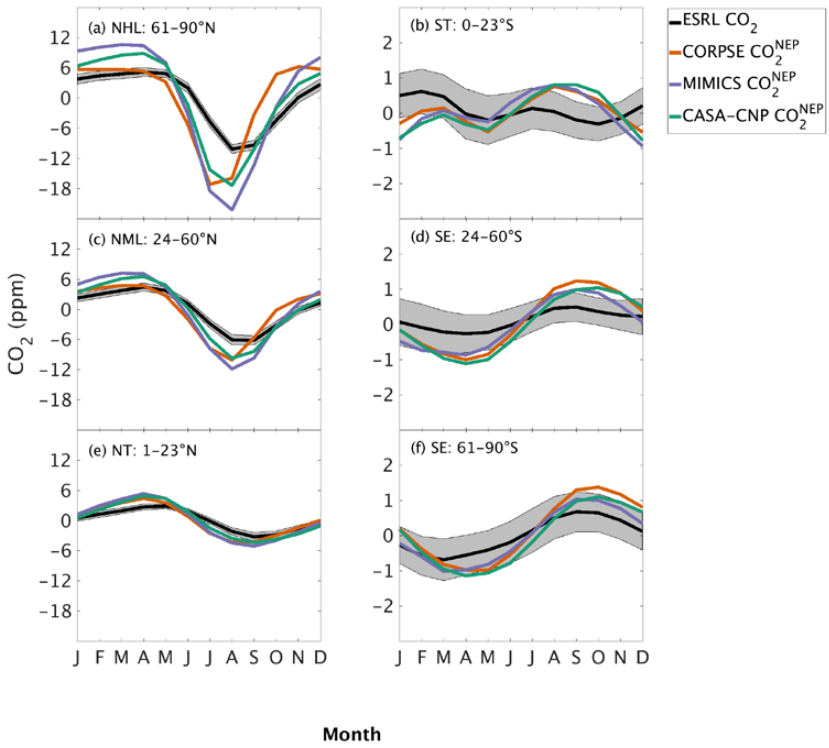

Figure 3. Climatological annual cycle (median) of CO_2 for observations (black) and global net ecosystem productivity flux (CO_2^{NEP}, colors) between 1982 and 2010 for six atmospheric sampling bands in the Northern Hemisphere (a-c) and Southern Hemisphere (d-f). Note the change in y-axis scale between the two hemispheres. Shading on the observed line represents one standard deviation due to interannual variability in the seasonal cycle.

https://doi.org/10.5194/bg-2019-256
Preprint. Discussion started: 15 July 2019

Biogeosciences Discussions
Open Access

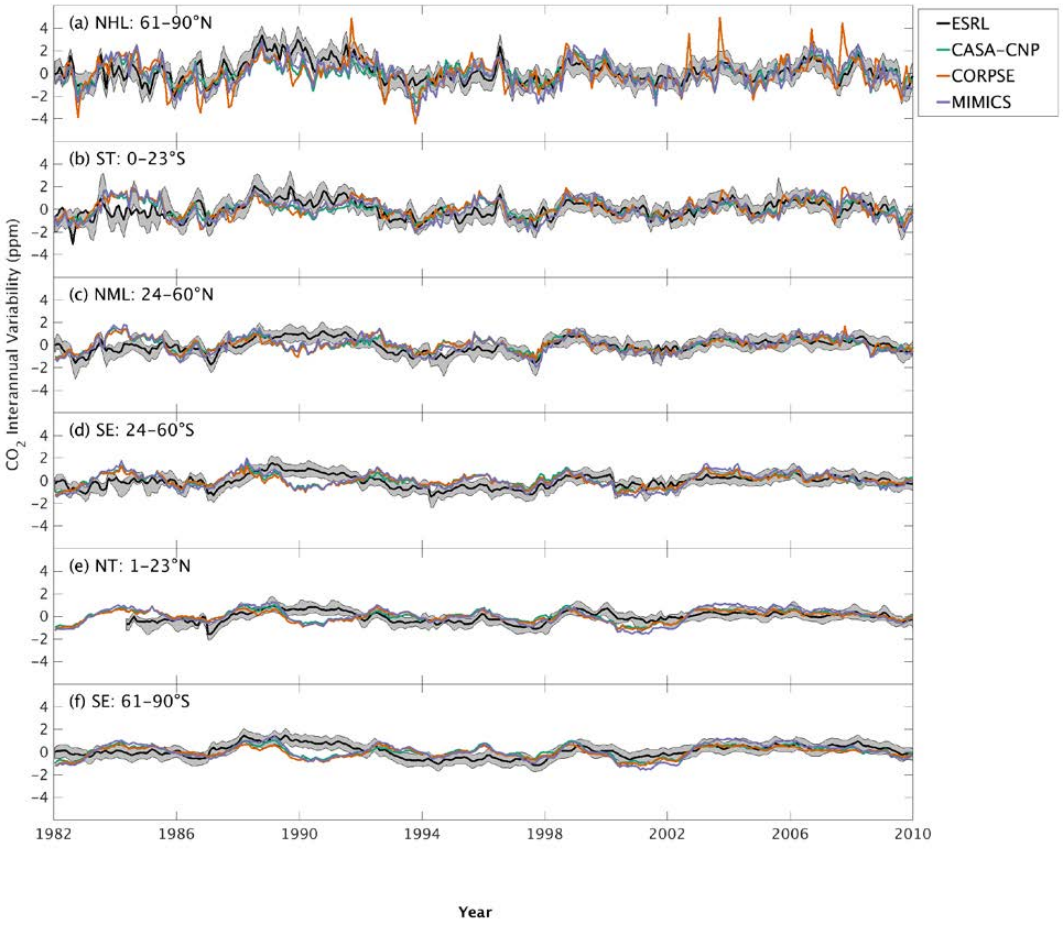

Figure 4. Interannual variability of CO_2 from global net ecosystem productivity (CO_2^{NEP} IAV) for testbed models (colors) and marine boundary layer observations from the NOAA ESRL network (black). Gray shading outlines one standard deviation of observed CO_2 interannual variability. High-latitude, mid-latitude and tropical land belts are shown for the Northern Hemisphere (a-c) and Southern Hemisphere (d-f).

https://doi.org/10.5194/bg-2019-256
Preprint. Discussion started: 15 July 2019

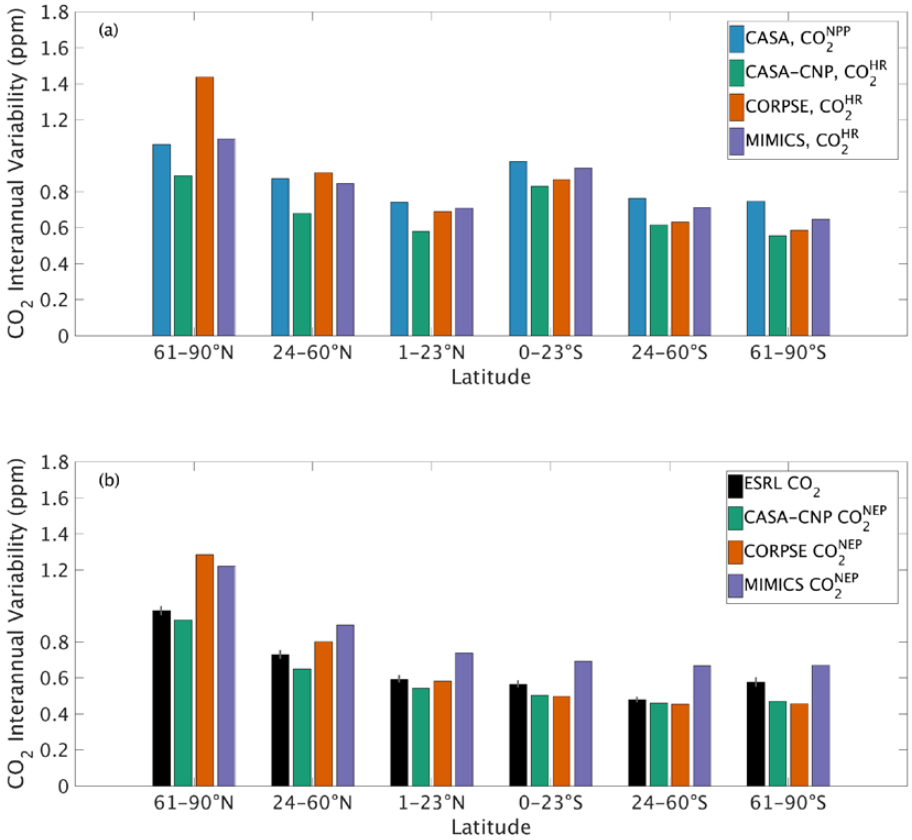

Figure 5: Magnitude of CO_2 interannual variability resulting from (a) individual flux components (CO_2^{NPP} IAV, CO_2^{HR} IAV) and (b) global net ecosystem productivity (CO_2^{NEP} IAV). Observed CO_2 IAV from NOAA ESRL network are shown with black bars whereas colors represent simulated data. Errorbars shown on the observed IAV represent two standard deviations, calculated as the median magnitude after removing a 12 month sliding window from the IAV timeseries.

https://doi.org/10.5194/bg-2019-256
Preprint. Discussion started: 15 July 2019

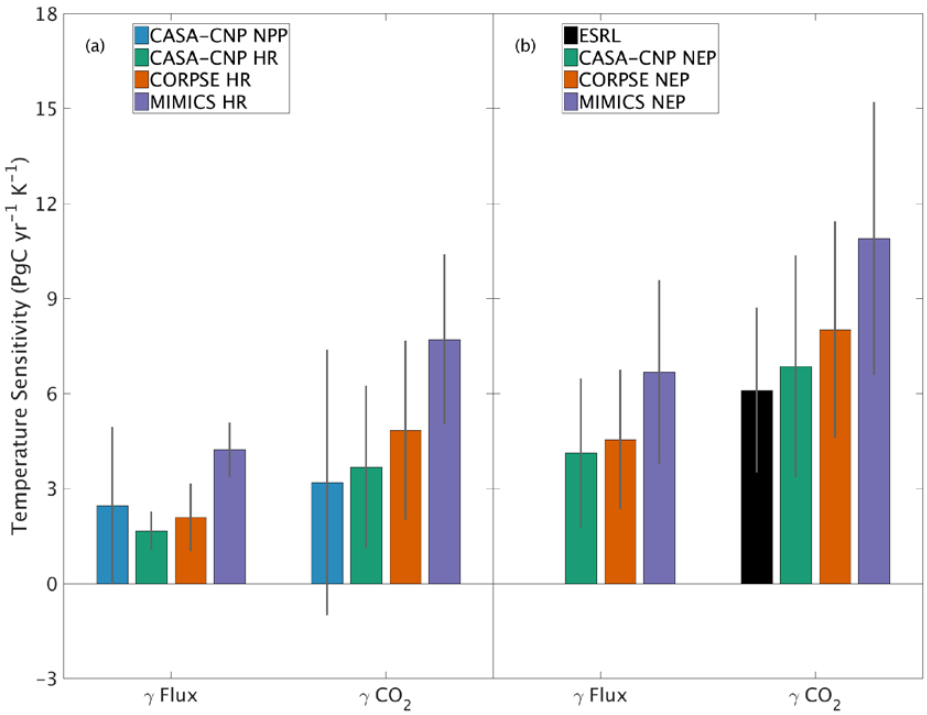

Figure 6: Temperature sensitivity (γ) calculated for interannual variability (IAV) of CASA-CNP air temperature and (a) flux IAV and corresponding CO_2 growth rate anomalies, (b) NEP IAV and CO_2^{NEP} growth rate anomalies. Reference sensitivity value (black) was calculated using NOAA ESRL CO_2 and CRU TS4 air temperature. Sensitivity values were calculated as the ordinary linear regression coefficient between IAV timeseries for 1982 to 2010. Errorbars represent the 95% confidence interval for coefficient values.

https://doi.org/10.5194/bg-2019-256
Preprint. Discussion started: 15 July 2019

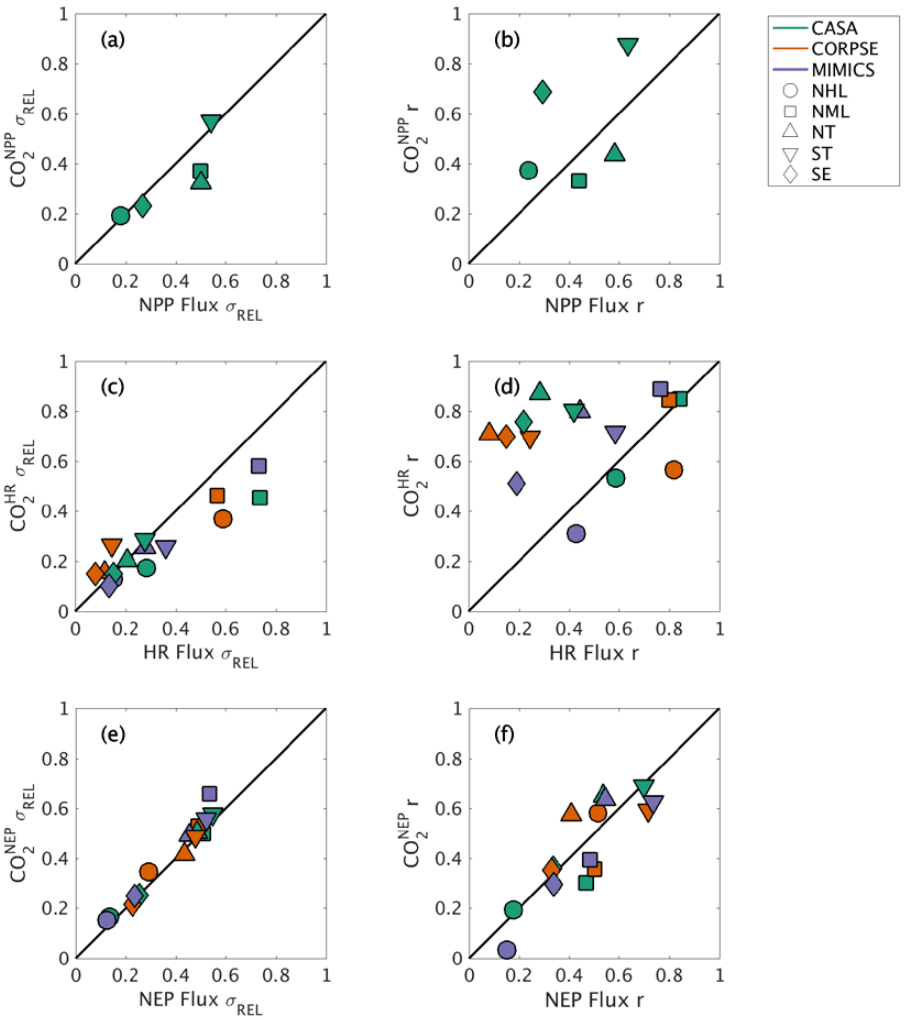

Figure 7: Comparison of regional and global interannual variability (IAV) from land fluxes and resulting atmospheric CO_2 between 1982 and 2010. (a, c, e) Normalized ratio taken between regional IAV and global IAV magnitude. (b, d, f) Linear correlation between regional IAV and global IAV. The scatterplot shows a direct comparison of ratio and correlation values for land flux values (x-axes) and corresponding CO_2 (y-axes). Shapes denote the source regions for both land fluxes and CO_2 response.